This is a repository copy of *Time-resolved visualization of the magnetization canting induced by field-like spin-orbit torques*.

White Rose Research Online URL for this paper:
https://eprints.whiterose.ac.uk/167486/

Version: Accepted Version

Time-resolved visualization of the magnetization canting induced by field-like spin-orbit torques

Simone Finizio,[1, *] Sebastian Wintz,[2] Sina Mayr,[1, 3] Alexandra J. Huxtable,[4] Manuel Langer,[1] Joe Bailey,[1, 5] Gavin Burnell,[4] Christopher H. Marrows,[4] and Jörg Raabe[1]

[1]*Paul Scherrer Institut, 5232 Villigen PSI, Switzerland*

[2]*Max-Planck-Institut für Intelligente Systeme, 70569 Stuttgart, Germany*

[3]*Laboratory for Mesoscopic Systems, Department of Materials,*
ETH Zurich, 8093 Zurich, Switzerland

[4]*School of Physics and Astronomy,*
University of Leeds, Leeds LS2 9JT, United Kingdom

[5]*École Polytechnique Fédérale de Lausanne (EPFL), 1015 Lausanne, Switzerland*

(Dated: October 27, 2020)

Abstract

We report on the use of time-resolved scanning transmission X-ray microscopy imaging for the visualization of the dynamical canting of the magnetization induced by field-like spin-orbit torques in a perpendicularly magnetized microwire. In particular, we show how the contributions to the dynamical canting of the magnetization arising from the field-like spin-orbit torque can be separated from the heating-induced effects on the magnetization of the microwire. This method will allow for the imaging of the dynamical effects of spin-orbit torques in device-like structures and buried layers.

An increasingly large part of the research in the field of spintronics is being dedicated to the developments of methods to control the magnetic configuration of a material using electrical currents. This research has first been focused on the study of well-established effects such as the spin-transfer-torque mechanism [1], which has e.g. allowed for the displacement of magnetic domain walls by purely electrical currents, leading to the proposal of various spintronic devices such as e.g. the magnetic racetrack memory [2]. However, since then an alternative approach has been discovered. This is based on current-induced spin-orbit torques (SOTs), which have been observed in multilayered heterostructures comprised of a ferromagnetic layer in contact with a heavy metal layer such as e.g. Pt or Ta [3–5], where a strong spin-orbit coupling between the electrons in the heavy metal layer and the ones in the ferromagnetic layer is present [6]. The flow of an electrical current across the heavy metal layer leads, as a consequence of the spin-orbit coupling between the electrons in the two layers to two effects, namely the spin Hall effect and the Rashba effect [6, 7].

The spin Hall effect gives rise, in the heavy metal layer, to a spin current perpendicular to the direction of the applied electrical current. This leads to an accumulation of spins of a given orientation at the interface between the heavy metal and the ferromagnetic layer, which then diffuse into the ferromagnetic layer, generating a spin-transfer torque [7]. Instead, the Rashba effect leads to a spin accumulation inside the ferromagnetic layer, as well generating a torque on the magnetization [7]. The combined torques generated by the spin Hall and Rashba effects are collected into the term SOTs. The SOTs can be categorized into two torques, described by effective magnetic fields applied on the ferromagnetic layer, under the names of field-like (FL) torque and damping-like (DL) torque [3, 4, 6–8]. Under the macrospin approximation [3, 4, 8], the FL-torque is proportional to $\mathbf{M} \times \mathbf{m}$, while the DL-torque is proportional to $\mathbf{M} \times (\mathbf{m} \times \mathbf{M})$, with $\mathbf{M}$ being the local magnetization vector of the ferromagnet, and $\mathbf{m}$ the vector describing the orientation of the spin magnetic moments diffusing into the ferromagnetic layer from the heavy metal layer.

For the development of devices based on the use of SOTs, the measurement of the torques induced by the injection of a current across the ferromagnet/heavy metal heterostructure is, together with the study of the dynamics of the SOTs, of vital importance. Various techniques, based e.g. on magneto-optical effects [9] and on electrical transport measurements [10, 11] have been employed for this purpose. Here, we present another technique, relying on synchrotron-based transmission X-ray imaging, offering the possibility to investigate the dy-

namics of the injected torques in device-like structures and in buried layers. This additional possibility is due to the longer penetration depth of X-rays if compared to visible light. For example, the attenuation length of X-rays tuned to the L_3 absorption edge of Co (ca. 778 eV) is of about 50-60 nm for the heavy metal materials used to generate the SOTs (e.g. Pt), and of about 400 nm for copper, used for the electrical contacting of the magnetic structures [12]. Both of those attenuation lengths are sufficiently large to guarantee the possibility to investigate the typical SOT multilayer stacks in transmission.

Synchrotron-based X-ray microscopy allows, thanks to the nanometer wavelength of X-rays and to the intrinsically pulsed structure of the X-rays generated by the synchrotron the possibility to perform time-resolved imaging with high temporal and spatial resolutions. Amongst the various pump-probe X-ray microscopy techniques, scanning transmission X-ray microscopy (STXM) is of particular interest. This is due to the fact that STXM allows for the use of a point detector for the measurement of the transmitted photon flux. For the acquisition of time-resolved images, a fast avalanche photodiode (i.e. with a recovery faster than the time between two consecutive electron bunches - 2 ns for the Swiss Light Source) is employed as the X-ray detector. Thanks to the fact that X-ray photons generated by neighboring electron bunches can be temporally resolved by this detector, it is possible to utilize the X-rays generated by the entire filling pattern of the synchrotron (in contrast to the use of a single electron bunch), leading to a reduction of up to two orders of magnitude in the time required to record a time-resolved image if compared to the standard pump-probe techniques [13, 14].

STXM is a transmission microscopy technique that, in its simplest configuration, illuminates the sample with an X-ray beam oriented perpendicular to the surface of the sample. The X-ray beam is focused by a Fresnel zone plate (FZP) to a spot on the surface of the sample. The dimension of the X-ray spot depend on the width of the outermost zone of the FZP and a beam diameter on the order of 25-50 nm is typically used. According to the X-ray magnetic circular dichroism (XMCD) effect, the magnetic sensitivity when illuminating the sample perpendicular to its surface is limited to the out-of-plane component of the magnetization, or M_z. A necessary question to ask for the feasibility of using STXM for the investigation of the SOTs is then if it is possible to quantitatively determine the effect of the SOTs on the magnetization by only measuring their out-of-plane component. In this manuscript, we will concentrate our attention on the FL-torque, as it is possible to isolate

it thanks to its odd symmetry with respect to the inversion of the magnetization direction.

For this discussion, let us consider two out-of-plane domains with opposite orientations, which we represent, using the macrospin approximation, as two magnetic moments with opposite orientation (see Fig. 1). Let us start by considering only the influence of the FL-torque on the two macrospins. Under this approximation, the FL-torque is proportional to $\mathbf{M} \times \mathbf{m}$. Therefore, the application of the FL-torque will lead to an in-plane canting of the two spins along the axis parallel to the direction of the injected current. This canting is described by the canting angle θ_S shown in Fig. 1. Given the fact that the two macrospins have opposite orientations, the sign of the M_x component will be opposite for the two magnetic moments. Therefore, in absence of other effects, the FL-torque would lead to a reduction of the M_z component of the two macrospins, and its dynamics could be measured by time-resolved STXM simply by determining the time-resolved change in the z component of the magnetic contrast during the application of the SOT pulse.
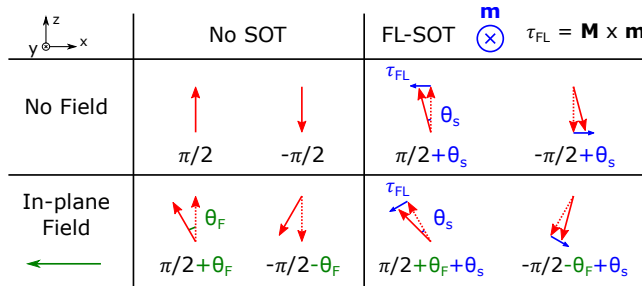

Figure 1. Schematic overview of the effect of the FL-torque on the spins in a continuous PMA domain in absence and presence of an in-plane magnetic field. In absence of both in-plane field and FL-torque, the spins in the PMA domains point either up or down (angle of $\pm\pi/2$ with respect to the surface plane). If the FL-torque (direction marked by the blue arrows) is applied, the two macrospins will cant of an angle θ_S, causing an equal reduction of the M_z component for the two macrospins. However, if an in-plane magnetic field is added, the spins will cant of an angle θ_F along the direction of the applied in-plane magnetic field (marked by the green arrow). The sign of this additional angle will depend on the original orientation of the spins. Therefore, if the FL-torque is now applied, the M_z component of the two macrospins will now be different, allowing for the extraction of the canting angle θ_S due to the FL-torque.

Let us now relax the stringent assumptions set in the previous paragraph, and consider the contribution of other effects that occur in the magnetic material when injecting the current

pulse generating the SOTs. In particular, let us now introduce the contributions arising from the DL-torque and from the heating induced by the current pulse. The DL-torque, under the macrospin approximation, gives rise to a torque proportional to $\mathbf{M} \times (\mathbf{m} \times \mathbf{M})$. Similarly to the case of the FL-torque, the DL-torque gives rise to an in-plane canting, but this time along the axis perpendicular to the direction of the injected current (y axis in Fig. 1). This canting angle θ_D, opposite for the two macrospin orientations (i.e. M_y is the same for both orientations), gives rise to the same reduction of the M_z component for the two macrospins. Furthermore, the injection of an electrical current across the microwire will generate an Oersted field (along the y axis), which will cause an additional tilting of the macrospins of a canting angle θ_Oe, opposite for the two macrospin orientations (i.e. M_y is the same for both orientations), giving as well rise to the same reduction of the M_z component for the two macrospins. Finally, the heating caused by the injection of the current pulse will cause a reduction of the saturation magnetization of the magnetic material, which will manifest, in the macrospin approximation, as a reduction of the length of the two spins, therefore resulting as well in a reduction of the M_z component.

Therefore, in absence of external biasing fields, both spin-orbit torques, the Oersted field, and the heating caused by the current pulse generating the torques will lead to a reduction of the M_z component for the two perpendicularly magnetized domains. As the four contributions all have the same response on ΔM_z, it is effectively impossible to separate one from the other, making the measurement of the spin-orbit torques impossible in this configuration.

To separate these four contributions, we propose to apply an in-plane magnetic field bias along the axis parallel to the direction of the injected current. Under the macrospin approximation, the effect of this biasing field can be described by an in-plane canting of the perpendicularly magnetized macrospins along the direction of the applied field. This canting is depicted in Fig. 1 by the angle θ_F. In this case, the sign of the angle is opposite for the two macrospins, as they both cant towards the same direction. Let us now inject the current pulse causing the SOTs, and analyze the effect of each of the contributions described above. The FL-torque will, again, cause a canting of the two macrospins of an angle θ_S along the axis parallel to the injected current. Under the assumption of a small canting angle caused by the FL-torque, this angle will be summed to the canting angle θ_F caused by the in-plane field, of opposite orientation for the two macrospins. Therefore, the total canting angle
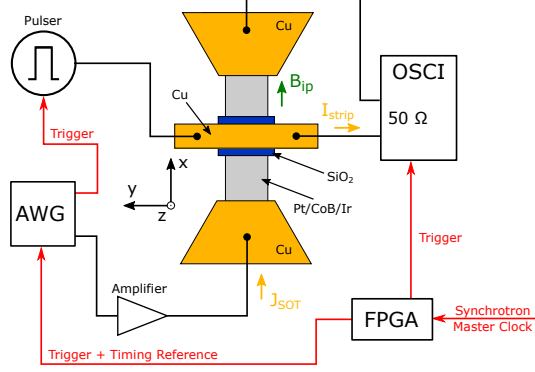
Figure 2. Schematic overview of the Pt/CoB/Ir microwire sample employed for the time-resolved measurement of the canting induced by the FL-torque and of the electrical setup used for the pump-probe experiments. The timing and synchronization signals are marked in red. J_{SOT} marks the path of the current pulse employed to generate the SOTs, and I_{strip} marks the path of the current pulse employed for the generation of the two opposite PMA domains in the Pt/CoB/Ir microwire. The direction of the applied in-plane magnetic field is indicated by the green arrow in the figure, and the coordinate system employed here is also marked in the figure.

along the axis parallel to the current direction will be of $\theta_S \pm \theta_F$ for the two oppositely oriented macrospins. The DL-torque and the Oersted field will cause the canting of the two macrospins along the axis perpendicular to the current direction of an angle $\theta_D + \theta_{Oe}$ for both of the macrospins. Finally, the heating caused by the injection of the current pulse will cause a reduction of the magnitude of the two macrospins.

Therefore, applying the superposition principle, the following relation will be valid for the two macrospins:

$$M_x^2 + M_y^2 + M_z^2 = M^2,$$
$$M^2 \sin^2(\theta_S \pm \theta_F) + M^2 \sin^2(\theta_D + \theta_{Oe}) + M_z^2 = M^2,$$

with M being the total magnitude of the two macrospins.

Defining m_i as the normalized magnetization along the i-th direction (i.e. $m_i = M_i/M$), it is possible to calculate that the magnitude of the canting angle θ_S caused by the FL-torque is given by the following relation:

6

(a)

ROI - ROI +

(b)

J_{SOI}

y
x
z

1 µm
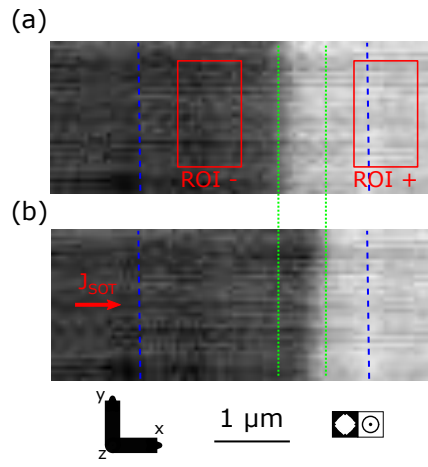
of the canting induced by the FL-torque, we have carried out such measurements on a 2 μm wide microwire patterned out of a Ta(2.7nm)/Pt(2.5nm)/[Co$_{68}$B$_{32}$(0.9nm)/Ir(0.4nm)/Pt(1.3nm)]$_{\times 3}$/Pt(2.1nm) multilayer stack (from now on referred to as Pt/CoB/Ir) exhibiting both PMA and interfacial Dzyaloshinskii-Moriya interaction, allowing for the stabilization of Néel-type domain walls [15]. The microwire was fabricated on top of a 200 nm thick X-ray transparent Si$_3$N$_4$ membrane on a 200 μm thick high resistivity Si frame. The patterning was performed by electron-beam lithography followed by lift-off of the Pt/CoB/Ir multilayer stack (details on the deposition of the Pt/CoB/Ir stack can be found in Refs. [15, 16]). To inject the current pulses across the Pt/CoB/Ir stack, the microwire was contacted by 200 nm thick Cu electrodes fabricated by electron-beam lithography followed by lift-off. To nucleate two PMA domains of opposite orientations on the microwire, a 400 nm thick Cu stripline was fabricated on top of the microwire, again by electron-beam lithography followed by a lift-off process. The microwire and the Cu stripline were electrically insulated by a 200 nm thick SiO$_2$ layer deposited between the microwire and the stripline. A schematic overview of the sample, along with an overview of the electrical setup employed for its excitation, is shown in Fig. 2. More details about the fabrication processes used for the samples reported here are given in Refs. [15–17].

The time-resolved measurements presented in this work have been carried out in the pump-probe regime using TR-STXM. In order to measure the dynamics of the canting of the spins caused by the FL-torque using Eq. (1), the Pt/CoB/Ir microwire was initialized in a bi-domain state by the injection of a 4 ns long, 350 mA current pulse across the Cu stripline shown in Fig. 2. The time-resolved measurements were then performed with the following protocol, which guaranteed the reproducibility of the dynamical processes necessary for pump-probe measurements: (i) a 20 ns long current pulse with a current density of 7.5×10^{11} A m^{-2} was injected across the Pt/CoB/Ir microwire, causing the SOT-induced canting of the two PMA domains, and a current-induced motion of the domain wall (CIDWM) between the two PMA domains [15, 17]; (ii) after 500 ns from the end of the first pulse, a 20 ns long current pulse with a current density of -7.5×10^{11} A m^{-2} was injected across the Pt/CoB/Ir microwire, causing the SOT-induced canting of the two PMA domains (in the opposite direction with respect to (i)), and the CIDWM of the domain wall back to its original position; (iii) after 700 ns from the end of the second current pulse, a 4 ns long, 350 mA current pulse was injected across the Cu stripline. This pulse is injected to

guarantee that the magnetic configuration is reset to the exact same state at each cycle. The first pulse, described in step (i), is injected 800 ns after the magnetic field pulse, leading to a total duration of one cycle of excitation of 2 μs. The long intervals between the pulses were selected to allow the microwire sufficient time to cool down before the injection of the next pulse.

The TR-STXM investigations were performed with a spatial resolution of 50 nm, and with a time step of 2 ns, using a prototype STXM and ptychography endstation currently under development at the SIM (X11MA) beamline of the Swiss Light Source [18]. The SIM beamline is equipped with two twin undulators [19], allowing for the generation of X-rays at the Co L_3 edge with pure circular polarization by operating the undulators at their first harmonic. To quantitatively determine both the static canting angle of the two PMA domains caused by the applied in-plane magnetic field and the dynamical canting of the spins in the two domains caused by the SOTs, all of the TR-STXM images presented in this work have been acquired with both circular left and right polarizations, allowing us to calculate the X-ray magnetic circular dichroic (XMCD) images. Given the orientation of the sample (perpendicular to the X-ray beam), the TR-XMCD images so obtained allow us to determine the z component of the magnetization vector, therefore enabling us to directly employ Eq. (1) for the calculation of the dynamical canting angle induced by the FL-torque.

To determine the canting of the PMA domains induced by the in-plane field, we acquired quasi-static XMCD images of the two PMA domains both with and without the in-plane field. From the ratio in the XMCD contrast between these two configurations, we could determine that an applied field of 115 mT leads to a canting θ_F of the PMA domains of about 30° away from the surface normal.

From the time-resolved XMCD-STXM images (videos of the time-resolved scans are shown in the supplementary information), we could extract the time-resolved variation of the magnetization in the two PMA domains during the application of the current pulses. The regions of interest used for extracting the time traces are shown in Fig. 3 (note here that the Pt/CoB/Ir microwire is buried below a thick Cu and SiO$_2$ layer). Those time traces are shown in Fig. 4. As shown in Fig. 4(a), the injection of a current pulse across the Pt/CoB/Ir microwire causes a visible variation in the XMCD contrast. This variation is due to the combination of the canting induced by the SOTs and the reduction of the saturation magnetization caused by the heating of the microwire [16]. The contribution arising from

9

the SOTs needs to be extracted from the total signal.

As shown in Fig. 4(b), if no in-plane field is applied, the time-resolved response of the magnetic contrast is equal within the measurement error for both orientations of the PMA domains. However, if an in-plane field is applied, as shown in Fig. 4(c), a different response is observed depending on the orientation of the PMA domain. This, according to the model introduced earlier, and schematically shown in Fig. 1, is attributed to the contribution of the FL-torque, and this contribution can be extracted from the time-resolved variation of the z component of the magnetization according to Eq. (1). The result of such analysis is shown in Fig. 5, where the calculated angle of the FL-torque is displayed.

From the time dependence of the canting angle induced by the FL-torque shown in Fig. 5, it is possible to observe that a maximum canting angle of 1.5±0.5° can be observed, and that the sign of the canting angle inverts, as would be expected, when inverting the direction of the current pulse. While Eq. (1) should account for the effect of the reduction of M_z due to the heating of the Pt/CoB/Ir microwire induced by the current pulse, we verified that this statement holds by observing that, when no pulse is applied to the microwire but where the heating effects are still present, no canting angle arises according to the calculations from Eq. (1), as shown in the supplementary information.

From the canting angle shown in Fig. 5, it is then possible to estimate, using a coherent rotation model [20], the effective field generated by the FL-SOT that would result in such a canting of the magnetization. Utilizing a value of 1.14 MA m^{-1} for the saturation magnetization and of 600 kJ m^{-3} for the perpendicular magnetic anisotropy for the Pt/CoB/Ir multilayer presented here [17], an effective field of 26±6 mT for the FL-SOT at an injected current density of 7.5×10^{11} A m^{-2} can be calculated. This value is consistent with the values for the FL-SOT effective magnetic field determined for other material systems using electrical transport measurement techniques [21], providing another indication of the applicability of TR-STXM for the investigation of SOT processes.

In conclusion, we have shown in this manuscript that TR-STXM can be employed for the quantitative investigation of the canting of the local magnetization induced by the FL-torque generated by the injection of a current pulse across a microwire fabricated out of a Pt/CoB/Ir multilayered stack, and for the indirect determination of the effective magnetic fields generated by the FL-torque acting on the CoB layer. The visualization of the FL-torque induced canting requires, in order to be able to separate it from the contributions

of the DL-torque and of the Joule heating, the application of an in-plane magnetic field to provide a symmetry breaking. With this technique, thanks to the longer penetration depth of X-rays in metals if compared to visible-light optical techniques, it will be possible to investigate the SOTs in device-like structures and in buried layers.

DATA AVAILABILITY STATEMENT

The data that support the findings of this study are openly available in the Research Data Leeds Repository at [[link to be added at the proof stage]].

ACKNOWLEDGMENTS

---

* Corresponding Author: simone.finizio@psi.ch

[1] D. Ralph and M. Stiles, Journal of Magnetism and Magnetic Materials **320**, 1190 (2008).

[2] S. Parkin and S.-H. Yang, Nature Nanotechnology **10**, 195 (2015).

[3] L. Liu, C.-F. Pai, Y. Li, D. C. Ralph, and R. A. Buhrman, Science **336**, 555 (2012).

[4] I. M. Miron, K. Garello, G. Gaudin, P.-J. Zermatten, M. V. Costache, S. Auffret, S. Bandiera, B. Rodmacq, A. Schuhl, and P. Gambardella, Nature **476**, 189 (2011).

[5] K. Garello, C. O. Avci, I. M. Miron, M. Baumgartner, A. Ghosh, S. Auffret, O. Boulle, G. Gaudin, and P. Gambardella, Applied Physics Letters **105**, 212402 (2014).

[6] P. Gambardella and I. Miron, Philosophical Transactions of the Royal Society A **369**, 3175 (2011).

[7] J. Sinova, S. O. Valenzuela, J. Wunderlich, C. H. Back, and T. Jungwirth, Reviews of Modern Physics **87**, 1213 (2015).

[8] M. Baumgartner, K. Garello, J. Mendil, C. O. Avci, E. Grimaldi, C. Murer, J. Feng, M. Gabureac, C. Stamm, Y. Ackermann, S. Finizio, S. Wintz, J. Raabe, and P. Gambardella, Nature Nanotechnology **12**, 980 (2017).

[9] C. Stamm, C. Murer, M. Berritta, J. Feng, M. Gabureac, P. M. Oppeneer, and P. Gambardella, Physical Review Letters **119**, 087203 (2017).

[10] C. O. Avci, K. Garello, A. Ghosh, M. Gabureac, S. F. Alvarado, and P. Gambardella, Nature Physics **11**, 570 (2015).

[11] H. Nakayama, M. Althammer, Y.-T. Chen, K. Uchida, Y. Kajiwara, D. Kikuchi, T. Ohtani, S. Geprägs, M. Opel, S. Takahashi, R. Gross, G. E. W. Bauer, S. T. B. Goennenwein, and E. Saitoh, Physical Review Letters **110**, 206601 (2013).

[12] B. L. Henke, E. M. Gullikson, and J. C. Davis, Atomic Data and Nuclear Data Tables **54**, 181 (1993).

[13] A. Puzic, T. Korhonen, B. Kalantari, J. Raabe, C. Quitmann, P. Jüllig, L. Bommer, D. Goll, G. Schütz, S. Wintz, T. Strache, M. Körner, D. Marko, C. Bunce, and J. Fassbender, Synchrotron Radiation News **23**, 26 (2010).

[14] S. Finizio, S. Wintz, B. Watts, and J. Raabe, Microscopy and Microanalysis **24**, 452 (2018).

[15] S. Finizio, S. Wintz, K. Zeissler, A. V. Sadovnikov, S. Mayr, S. A. Nikitov, C. H. Marrows, and J. Raabe, Nano Letters **19**, 375 (2019).

[16] S. Finizio, K. Zeissler, S. Wintz, S. Mayr, T. Weßels, A. J. Huxtable, G. Burnell, C. H. Marrows, and J. Raabe, Nano Letters **19**, 7246 (2019).

[17] S. Finizio, S. Wintz, S. Mayr, A. J. Huxtable, M. Langer, J. Bailey, G. Burnell, C. H. Marrows, and J. Raabe, Applied Physics Letters **116**, 182404 (2020).

[18] M. Langer, C. A. F. Vaz, S. Chiriotti, A. Bergamaschi, M. Guizar-Sicarios, A. Kleibert, and J. Raabe, Microscopy and Microanalysis **24**, 54 (2018).

[19] U. Flechsig, F. Nolting, A. Fraile Rodriguez, J. Krempasky, C. Quitmann, T. Schmidt, S. Spielmann, and D. Zimoch, AIP Conference Proceedings **1234**, 319 (2010).

[20] C. Tannous and J. Gieraltowski, European Journal of Physics **29**, 475 (2008).

[21] K. Garello, I. M. Miron, C. O. Avci, F. Freimuth, Y. Mokrousov, S. Blügel, S. Auffret, O. Boulle, G. Gaudin, and P. Gambardella, Nature Nanotechnology **8**, 587 (2013).
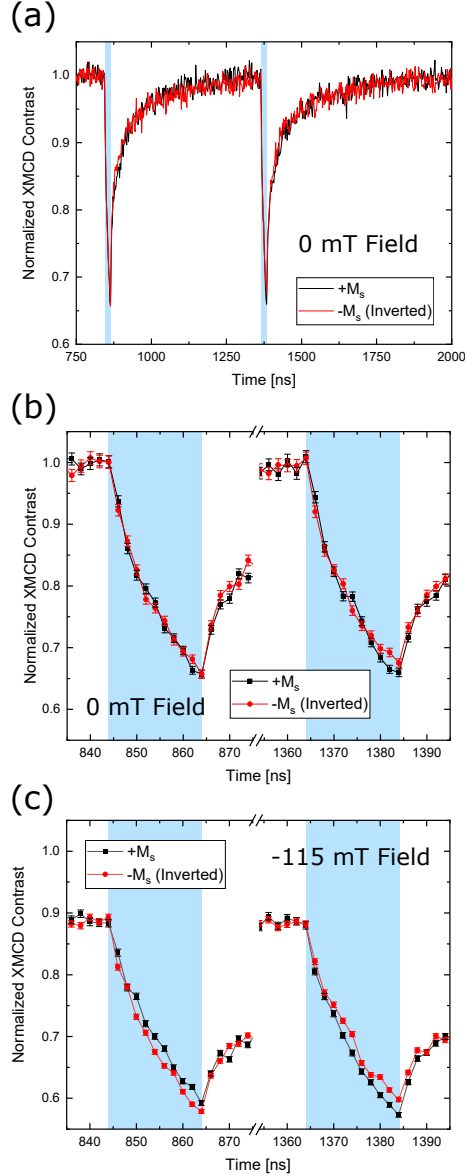
Figure 4. Time-resolved variation of the absolute value of the z component of the magnetization in the two PMA domains. The time steps where the pulses are applied are marked by the light blue background. (a) Time trace of the z component of the magnetization showing the injection of the positive and negative current pulses across the Pt/CoB/Ir microwire. A strong contribution to the dynamics of the z component of the magnetization is given by the heating caused by the injection of the current pulse. (b) Detail of (a), showing the regions where the current pulses are applied. No substantial differences can be spotted for the two PMA domains when no in-plane field is applied. (c) Time trace of the z component of the magnetization with an in-plane field of -115 mT applied. Here, a difference between the two PMA domains, attributed to the contribution of the FL-torque can be spotted.
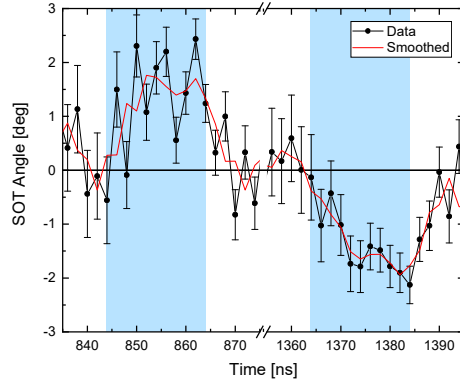
Figure 5. Calculated value of the canting angle induced by the FL-torque on the Pt/CoB/Ir microwire. A canting angle of about 1.5° can be observed, and a change in its sign can be observed when applying a pulse of opposite polarity. The time steps where the pulses are applied are marked by the light blue background. The red curve shows the time trace after a 3-point adjacent average smoothing.